

RESEARCH ARTICLE

Wi-ESP—A tool for CSI-based Device-Free Wi-Fi Sensing (DFWS)

Muhammad Atif , Shapna Muralidharan , Heedong Ko and Byounghyun Yoo *

Center for Imaging Media Research, Korea Institute of Science and Technology (KIST), 5 Hwarangro14-gil Seongbuk-gu Seoul 02792 South Korea

*Corresponding author. E-mail: yoo@byoo.net  <http://orcid.org/0000-0001-9299-349X>

Abstract

Recent progress in Device-Free Wi-Fi Sensing (DFWS) has established the use of wireless signals like Wi-Fi not only to communicate but also as a tool to enable device-free sensing. As an emerging technique, DFWS has many capable applications such as sensing activity and gesture and fall detection, monitoring elderly, surveillance, and many more applications while waiving out the necessity to mount devices on the object. A wide range of applications can use the channel state information (CSI) from commercial Wi-Fi devices pervasively for ubiquitous sensing. Existing CSI tools, such as the Intel 5300 network interface controller tool or the Atheros 9390 tool, have limitations when deployed in large-scale systems due to their high deployment costs and limitations in the resolution of CSI measurements. Due to these shortcomings, DFWS applications need an alternative CSI tool in order to perform efficiently. In this paper, we present ESP32-based Wi-ESP as a CSI gathering tool that can report detailed CSI measurements based on 802.11n standards. The proposed Wi-ESP tool works as a complete device by collecting the CSI measurements as well as processing further for DFWS applications. Wi-ESP can work as standalone device, unlike other CSI tools, and can offer large-scale deployment to many DFWS applications. In this paper, we have explored the options of Wi-ESP as a tool for CSI measurements and processing and propose it as a tool for DFWS.

Keywords: device-free Wi-Fi sensing (DFWS); RSSI; CSI; ESP32; Wi-ESP; applications

1. Introduction

Device-Free Wi-Fi sensing (DFWS) is becoming a popular research field due to the ubiquitous availability of Wi-Fi signals and comparatively accurate sensing with less infrastructure (Zhou, Wu, Yang, & Liu, 2015; Savazzi et al., 2016). The primary advantage of DFWS is the ability to exploit the Wi-Fi signals around us to detect a person, fall, gesture, location, and various other applications passively (Wang, Guo, Yu, & Zhou, 2018; Ren et al., 2019). Figure 1 illustrates the concept of DFWS. In comparison with state-of-the-art techniques using sensors, cameras, or wearables to monitor an environment or a person, DFWS uses

Wi-Fi signal patterns to sense the state. The main advantage of being device free is that it does not require installing sensors or cameras to measure the states directly. After receiving the sensed raw samples and filtering them, the values can be used for behavior estimation using machine learning and big data techniques. DFWS can be an ideal solution for many applications such as the Internet of Things (IoT), human activity recognition, and monitoring elderly people, since it is less obtrusive and offers pervasive sensing. The earliest work on “Sensorless Sensing” was a human sensing application using wireless sensor networks and a received signal strength indicator (RSSI)-based detection by Youssef et al. (Woyach, Puccinelli, &

Received: 7 February 2020; Revised: 25 March 2020; Accepted: 16 April 2020

© The Author(s) 2020. Published by Oxford University Press on behalf of the Society for Computational Design and Engineering. This is an Open Access article distributed under the terms of the Creative Commons Attribution Non-Commercial License (<http://creativecommons.org/licenses/by-nc/4.0/>), which permits non-commercial re-use, distribution, and reproduction in any medium, provided the original work is properly cited. For commercial re-use, please contact journals.permissions@oup.com

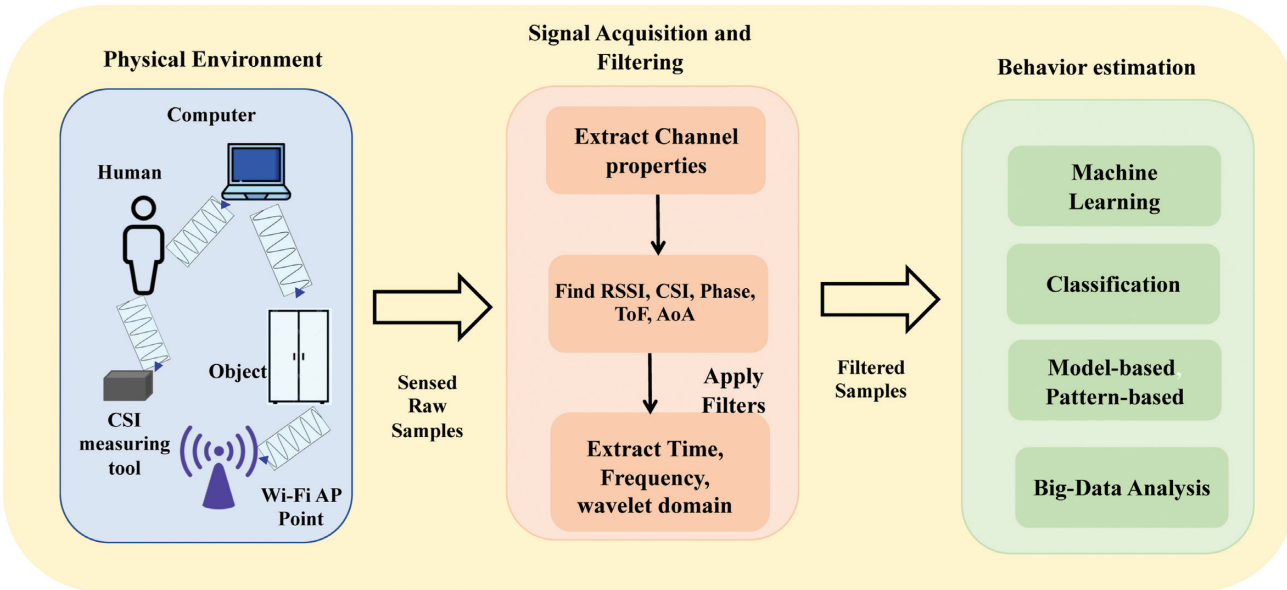


Figure 1: Concept of DFWS.

Haenggi, 2006; Youssef, Mah, & Agrawala, 2007). These preliminary works on localization and tracking the presence of humans accelerated the deployment of various applications based on DFWS. Unlike the use of RSSI, channel state information (CSI) in 802.11n gives more fine-grained access to the physical (PHY) layer and leverages useful information for DFWS applications.

Various applications in the past using DFWS have adopted RSSI to represent received power level at the receiver from wireless local area network (WLAN) 802.11b/n/c (Khalili, Soliman, Asaduzzaman, & Griffiths, 2019). However, the fact that the received signal power decreases with increasing distance from the source due to propagation loss in RSSI measurement, giving inaccurate values, is a limitation. Different RSSI values due to the multipath effect are another constraint. Current research works use CSI to overcome the possible disadvantages of using RSSI for DFWS. CSI is a fine-grained value from the PHY layer that details the amplitude and phase on each subcarrier in the radio frequency domain and is a different parameter from RSSI. In contrary to one RSSI for each packet, we receive multiple CSI values, making the DFWS more accurate. CSI has received more attention in recent years since it can be exported from devices having a wireless network interface controller (NIC; Halperin, Hu, Sheth, & Wetherall, 2011a). CSI has frequency diversity due to its multipath reflection, and contains more information than RSSI since it uses measurements per Orthogonal Frequency Division Multiplexing (OFDM) from each packet (Bhartia, Chen, Ralapalli, & Qiu, 2011; Yang, Zhou, & Liu, 2013). CSI thus represents a more reliable and precise model for DFWS.

Existing tools used to monitor CSI measurements in most of the current works include the Intel 5300 NIC tool (Halperin et al., 2011a) and Atheros 9390 (Xie, Li, & Li, 2018) tool with some additional enhancements. These CSI tools are usually equipped with a commodity router as the transmitter (TX) and devices such as a Personal Computer (PC) or any other devices with a Wi-Fi NIC card as the receiver (RX). CSI measurements using the existing tools have several practical limitations while applying in a variety of domain-specific applications. The first constraint includes the need for a laptop with a specific NIC to act as RX, with research studies needing up to 10 laptops on the RX side. The constraint mentioned above can be a limitation when we consider

the concept of DFWS with resource-constraint applications such as IoT. Realizing scalability and maintenance in large-scale systems that require specific devices is a downside offsetting the advantages of using CSI values. Another disadvantage of using the Intel 5300 NIC involves the resolution of CSI measurements, since it provides CSI for only 30 out of 52 subcarriers with a 20 MHz bandwidth for each TX-RX pair. The goal of obtaining accurate values might not be realized due to incomplete coverage of all subcarriers (Yang, Zou, Jiang, & Xie, 2018). Moreover, the CSI information received from the subcarriers is random, making it difficult to know from which subcarrier a particular signal is received. Specific applications such as breathing and heart rate monitoring need more accurate CSI measurements, which are possible if data from all the subcarriers are available. Recent studies upgrade the tools used for CSI measurements to overcome bottlenecks such as acquiring all the subcarriers, but still need multiple devices to accomplish DFWS.

Unlike the prevailing methods, our proposed DFWS framework relies on Wi-ESP as a tool for CSI measurement and processing. ESP32 implements Transmission Control Protocol/Internet Protocol (TCP/IP), full 802.11 b/g/n/e/i Wireless Local Area Network (WLAN) Medium Access Control (MAC) protocol, and can communicate with most Wi-Fi Routers in station (client) mode. It can also act as an Access Point (AP) with full 802.11 b/g/n/e/i WLAN MAC protocol, and can communicate to most of the Wi-Fi routers in station (client) mode. It can also act as an AP with full 802.11 b/g/n/e/i. ESP32 does not require any special TX or RX for CSI measurements as it can mimic both a TX and RX. The ESP32 tool gives accurate and richer channel information along with CSI measurements from all 52 subcarriers in the frequency domain for use in DFWS applications. In this paper, we have analyzed the possibilities of Wi-ESP as a CSI tool for DFWS applications. The proposed tool is evaluated for acquiring CSI specifically rather than proposing it as a solution for DFWS applications. The major contributions in this paper are:

- Analyzing the literature for possible advantages of using CSI values for DFWS applications from literature study
- Evaluating the Wi-ESP as a possible tool for CSI measurements

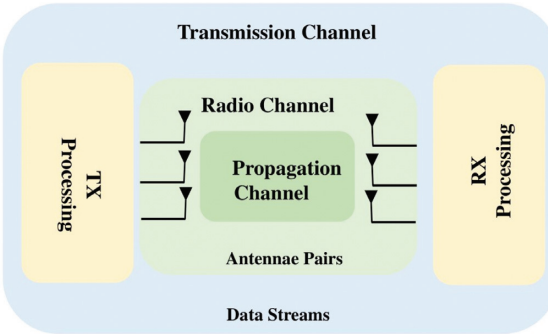


Figure 2: Concept of MIMO.

- Analyzing the CSI measurements from Wi-ESP for obtaining precise CSI values
- Proposing Wi-ESP as a possible CSI measurement tool for DFWS after evaluations

The remainder of the paper is organized as follows. Section 2 presents discussion of DFWS based on CSI and related work. Section 3 illustrates the capabilities and features of Wi-ESP. Section 4 explains the performance evaluation of Wi-ESP for CSI measurements to enable DFWS applications. Section 5 concludes the paper.

2. CSI-Based DFWS and Related Work

DFWS uses radio frequency (RF) signals and digital signal processing technology to enable pervasive sensing. DFWS collects information on a sensed environment, along with the modulated Wi-Fi signals, and uses it to identify various actions such as localization, movement detection, fall detection, and many other applications. In this section, we describe the OFDM in 802.11n before elaborating wireless sensing using CSI and then the existing literature work on DFWS.

2.1. OFDM in 802.11n

The performance of 802.11n depends on the PHY layer details of the RF channel. In addition to the RSSI values available in previous

	0	0	Time Domain Outputs
Null	1	1	
#1	2	2	
#2	.	.	
#26	26	26	
Null	27	27	
Null	.	.	
Null	37	37	
#-26	38	38	
.	.	.	
#-2	62	62	
# -1	63	63	

Figure 4: Inputs and outputs of inverse Fourier transform.

ous 802.11 versions, which provide coarse-grained information of channel properties and packet delivery, CSI values are available in 802.11n. In contrast to RSSI, CSI acquires amplitude and phase information for OFDM subcarriers between each TX and RX antennas pair. OFDM uses multiple subcarriers and provides high data rates up to 54 Mb/s (Cho, Kim, Yang, & Kang, 2010). Conceptually, in the multiple-input multiple-output (MIMO) system as shown in Fig. 2, for N_t TXs there will be N_t OFDM channels. Each channel produces its own OFDM symbol and receives N quadrature amplitude modulation symbols from the MIMO encoder. These N symbols are converted by an Inverse Fast Fourier Transform (IFFT) to the required OFDM in the time domain in the TX. The RX performs the inverse operation, where the OFDM symbols are converted back to the frequency domain by a Fast Fourier Transform (FFT; IEEE 802.11 Working Group, 2016). OFDM applies IFFT/FFT for modulation and demodulation to reduce the system complexity. Figure 3 illustrates the concept of signal processing in 802.11n.

The most common way to execute the inverse Fourier transform is by implementing the IFFT algorithm. For example, Fig. 4 shows an example of 64-point IFFT adoption. Coefficients of 1 to 26 are mapped to the same numbered IFFT inputs, while the coefficients -26 to -1 are mapped to IFFT inputs 38 to 63. The rest

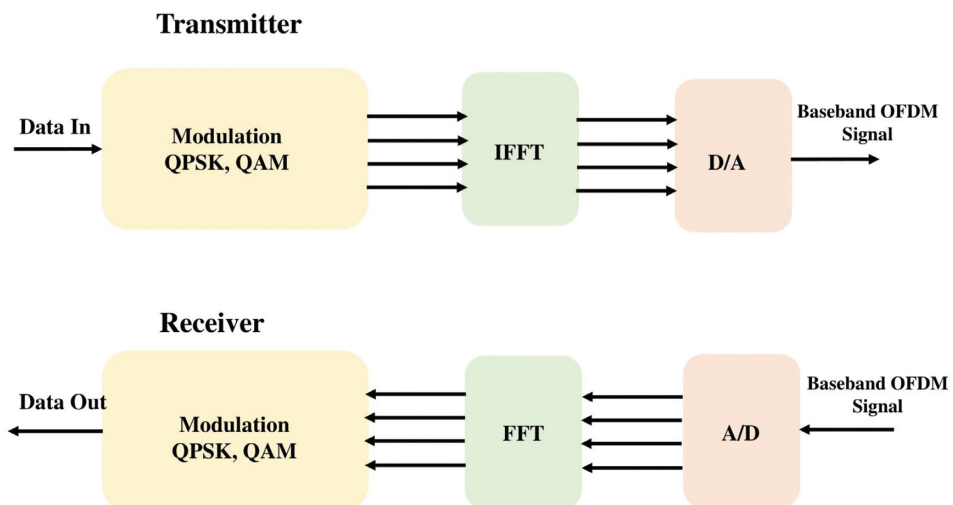


Figure 3: Illustration of signal processing in 802.11n.

of the inputs, 27 to 37, and the 0 (dc) input are set to 0. The IFFT algorithm cyclically calculates the output and maps the resulting waveform to the required OFDM symbol length (IEEE 802.11 Working Group, 2016).

2.2. Wireless sensing using CSI

CSI helps in estimating the channel properties of a communication link. Wireless signals propagating from TX to the RX are affected due to the presence of physical objects in an indoor environment, resulting in reflection, diffraction, and scattering (Wang, Wu, & Ni, 2016; Al-qaness et al., 2019). CSI provides information that describes how wireless signals propagate in the channel with the various effects such as time delay, amplitude attenuation, and phase shift on each subcarrier. Recent Wi-Fi devices embrace OFDM at the physical layer and follow the IEEE 802.11n/ac standard that permits multiple TX and RX antennas for MIMO communication. Each CSI value represents the channel frequency response (CFR) as in Equation (1) (Tse & Viswanath, 2005; Zhang, Liu, Lu, & Gong, 2018)

$$H(f; t) = \sum_n^N a_n(t) e^{j2\pi f \tau_n(t)}, \quad (1)$$

where $a_n(t)$ is the amplitude attenuation factor, $\tau_n(t)$ denotes the propagation delay, and f expresses the carrier frequency. The amplitude and phase of CSI are affected when there are physical changes in the surrounding environment (Zhang, Wang, & Wu, 2017). To calculate CSI, the Wi-Fi TX assigns long training symbols (LTFs), which possess pre-defined symbols for every subcarrier, in the packet preamble. When we obtain the LTFs, the Wi-Fi RX calculates the CSI matrix using the received signals and the original LTFs. For every subcarrier, the Wi-Fi channel is designed by $y = Hx + n$, where y is the signal received by RX, x is the signal transmitted from TX, H is the CSI matrix, and n is the noise vector. After receiving y , the RX calculates the CSI matrix H using x and the received signal y after eliminating the cyclic prefix, demapping, and OFDM demodulation. The final estimated CSI is a 3D matrix of complex values, which evaluates the channel quality using each entry of the matrix. Equation (2) represents the final CSI values (Ma, Zhou, & Wang, 2019)

$$H_i = H_{ie}^{j\angle H_i}, \quad (2)$$

where H_i and $\angle H_i$ are the amplitude and phase response of the i th subcarrier, respectively. Such sampling gives fine-grained information, smaller variation, and more accurate values. Behavior recognition, human activity recognition, localization, and many other applications based on DFWS have garnered much research attention currently due to the fine-grained CSI sensing and the fact that a variety of Wi-Fi devices are available indoors. Furthermore, since the CSI takes account of propagation path variation, it can be leveraged to show the changes caused by the physical environment. As a result, a variety of applications use CSI-based DFWS. Various existing tools modify the NIC driver to enable CSI, using the Intel 5300 NIC for example (Halperin, Hu, Sheth, & Wetherall, 2011b). Another popular implementation is the Atheros 9580 (Duan, Yu, & He, 2018; Xie et al., 2018) and its modifications including the Atheros AR9382 (Zhao et al., 2019), Atheros AR9462, AR9480 (Choi, Lee, Lee, Lee, & Kim, 2017), and Atheros 9390 (Sen, Lee, Kim, & Congdon, 2013; Zou et al., 2018) using their own state-of-the-art technologies. The related work based on these implementation tools is discussed below.

2.3. Related work

Some comprehensive literature reviews exist on general DFWS (Khalili et al., 2019), as well as reviews specific to human activity and behavior recognition (Al-qaness et al., 2019; Wang et al., 2019). Reviews of elaborate works such as applications like localization and gesture-free recognition are also prevalent (Yang et al., 2013; Wengrowski, 2014; Jiang, Zimu, Youwen, & Lionel, 2016; Wu, Zhang, Xu, Wang, & Li, 2017; Yousefi, Narui, Dayal, Ermon, & Valaee, 2017; Xin et al., 2018). All these works summarize on existing research based on its application, signal processing, noise reduction, signal transform, and signal extraction. Furthermore, existing reviews discuss works based on a modeling-based algorithm, learning-based algorithm, and hybrid algorithms (Gong et al., 2016). The reviews document applications based on detection, recognition, and estimation in elaborate detail. Since existing reviews provide a thorough survey on DFWS and its applications, we focus on the tools used in the existing studies. One of the most common tools used by applications is the Intel 5300. One of the shortcomings of the Intel 5300 NIC, as mentioned previously, is the provision of CSI for only 30 subcarriers out of 52 subcarriers with a 20 MHz bandwidth for each TX-RX pair.

Furthermore, deriving accurate CSI values from the NIC is demanding since the CSI has signal processing circuit properties in the baseband along with channel properties. Some studies have described errors in measuring CSI values due to imperfection in the wireless signal processing, including power control uncertainty, packet detection delay, sampling frequency offset, carrier frequency offset, random initial phase offset, and phase ambiguity (Zhuo, Zhu, Xue, & Chang, 2017). Moreover, due to hardware faults, there are other vulnerabilities such as packet detection delay, CSI amplitude offset due to power control ambiguity, and phase offset error in each subcarrier. Consequently, the CSI measurements can be inaccurate, leading to problems for applications relying on them (Tzur, Amrani, & Wool, 2015; Xie et al., 2018). Due to these shortcomings, this tool can be used for research purposes, but not for practical implementations (Yang et al., 2018). Another tool commonly used in DFWS applications is the Atheros-CSI tool (Xie et al., 2018). It is an open-source 802.11n measurement tool that facilitates extraction of detailed PHY wireless communication information from the Atheros Wi-Fi NICs. The main disadvantage of Atheros-CSI tool is that the implementation of the setup is complex, making it difficult to implement with many applications. Similar to the Intel 5300 device, the Atheros-CSI tool needs computers set up for the CSI measurements. Additionally, the raw phase measurements need calibration using a method such as linear transformation to obtain analyzable CSI data (Zhuo, Zhu, & Xue, 2016; Zheng, Hu, & Chen, 2018). DFWS applications include monitoring the elderly, human detection, and healthcare applications, which require more straightforward implementation. Furthermore, obtaining CSI values efficiently helps when implementing DFWS in large-scale scenarios such as IoT.

Along with the limitations of CSI tools mentioned above, there are other challenges pertaining to DFWS. Most of the studies have carried out experiments in a controlled environment. The results are different in real-world physical environments due to factors such as location of the RX, people, and so on. To overcome these shortcomings, we need a CSI tool to address the implementation challenges as well as the cost, with the ability to maintain the accurate CSI values required for DFWS. In this paper, we propose a Wi-ESP-based CSI tool to implement DFWS efficiently and overcome the challenges of existing tools.

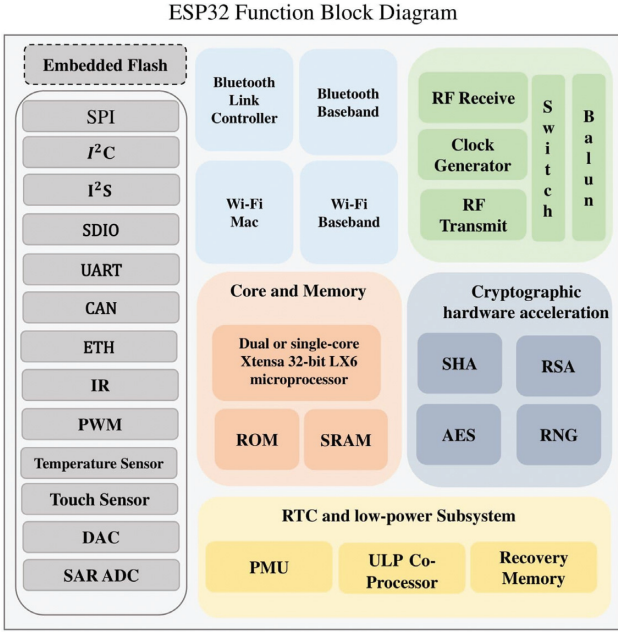


Figure 5: ESP32 functional block diagram.

3. Wi-ESP—A Proposed CSI Tool

ESP32, a successor of ESP8266, is created by Espressif Systems. It is a low-cost, low-power system on a chip series with both Wi-Fi and dual-mode Bluetooth functionalities (Espressif, 2020). ESP32 is highly integrated, with a dual-core 32-bit processor, and bundled with all necessary peripherals such as in-built antenna switches, RF balun, power amplifier, low-noise receiving amplifier, filters, sensors, and power management modules, as shown in Fig. 5. It has ultra-low power consumption, making it suitable for mobile devices, IoT applications, and wearables, since its state-of-the-art technology includes fine-grained clock gating, different power modes, and adaptive power scaling. ESP32 has a hybrid Wi-Fi and Bluetooth chip and can function as a standalone device. It can interface with other systems such as universal asynchronous receiver-transmitter (UART)/secure digital input output, or inter-integrated-circuit interfaces.

The ESP32 Wi-Fi driver can support various 802.11 b/g/n protocols and can work in station-only mode or AP-only mode, or both together. ESP32 Wi-Fi has a complete API reference and it is set up during the initialization process. The power-saving mode is either the standard modem sleep mode or a maximum power-saving mode. ESP32 can support up to 16 antennas through an external antenna switch. We can simultaneously enable only one or two antennas for RX/TX, but the antenna switch can connect up to four address pins.

CSI in ESP32 contains the channel frequency responses of subcarriers and is calculated when packets travel from TX to RX. Each CFR of a subcarrier registers as two bytes of signed characters, the first part being the imaginary, and the second part is the real value, and we receive three CFR types from the CSI information. The in-built specification in ESP32 is for three CFR types to be received from the CSI information. These are legacy long training field (LLTF), high-throughput LTF (HT-LTF), and space-time block code HT-LTF (STBC-HT-LTF). Channels receiving different types of packets with the different states, the subcarrier index, and total bytes of signed characters of CSI are shown in Table 1 (ESP-IDF Programming Guide 2020).

Table 1: Wi-Fi CSI information from different training fields.

Packet information	Secondary channel	None	Below			Above			HT	Non-HT	40 MHz	20 MHz	20 MHz	HT
			HT	Non-HT	HT	Non-STBC	STBC	Non-STBC						
Subcarrier index	STBC	Non-STBC	Non-STBC	STBC	Non-STBC	0~63	0~63	0~63	Non-STBC	STBC	Non-STBC	STBC	Non-STBC	STBC
	LLTF	0~31, -32~-1	0~31, -32~-1	0~31, -32~-1	0~31, -32~-1	-32~-1	-32~-1	-32~-1	-64~-1	-64~-1	-64~-1	-64~-1	-64~-1	-64~-1
	HT-LTF			0~31, -32~-1	0~31, -32~-1	0~31, -32~-1	0~31, -32~-1	0~31, -32~-1	0~62	0~62	0~62	0~62	0~62	0~62
STBC- HT-LTF									0~60, -60~-1	0~60, -60~-1	0~60, -60~-1	0~60, -60~-1	0~60, -60~-1	0~60, -60~-1
Total bytes	128	256	384	128	256	380	384	384	612	128	256	376	384	612

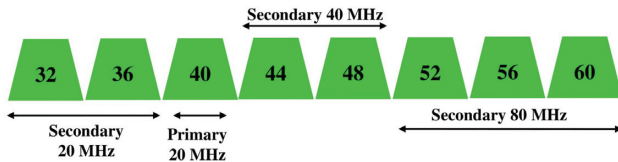


Figure 6: Illustration of secondary channels.

Wide bandwidth channels, such as 40, 80, and 160 MHz, consist of the primary 20 MHz channel and one or more secondary channels, as shown in Fig. 6 (ESP-IDF Programming Guide 2020). The first row of Table 1 outlines the presence of secondary channel details. The packet information explains the signal mode and the bandwidth parameters. The subcarrier details show the CSI values received from the different training fields LLTF, HT-LTF, and the STBC-HT-LTF. The final row explains the various sizes of the received CSI values from various training fields. All three training fields may not be present depending on the channel and packet information, as shown in Table 1. The training fields are chosen based on the DFWS deployment scenario. The buffer stores the CSI values as two parts, and the order in which they are stored is shown in Table 1. Depending on the channel and packet information, the values of LTF are available. We also receive useful information such as RSSI, noise floor of RF, and receiving time (ESP-IDF Programming Guide, 2020).

ESP32 supports Wi-Fi bandwidths of HT20 or HT40, but does not support the use of both simultaneously. Since ESP32 can function both as a station and an AP, the default bandwidth is HT40 for a station or AP. We carry out this setup during the initial tuning process of ESP32, but the setup can be negotiated while setting the connections between stations and AP. In the mode where station and AP coexist, each mode can configure

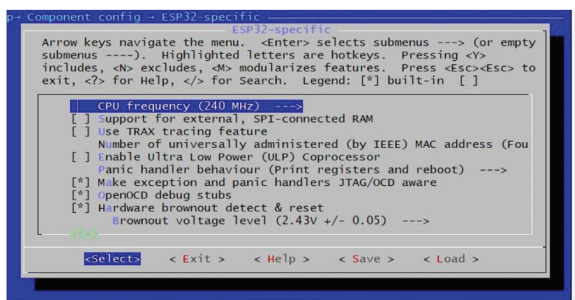
the channel bandwidth separately. When both of these coexist, the station has the highest priority than does AP in ESP32. The HT40 bandwidth has a higher throughput of about 150 Mbps, whereas HT20 has a bandwidth of 72 Mbps. Since ESP32 can support simultaneous AP and station mode, the entire setup for DFWS can be enabled, along with its processing power, to track CSI data in real time. The resulting CSI measurements do not contain random errors, and DFWS applications can use the information for gesture recognition, localization, etc. The specifications of ESP32 can facilitate the complete processing of CSI values in the device without the need for external devices, in contrast to the existing CSI tools. Wi-ESP implementation based on ESP32 works as a standalone device for DFWS applications.

4. Performance Evaluation

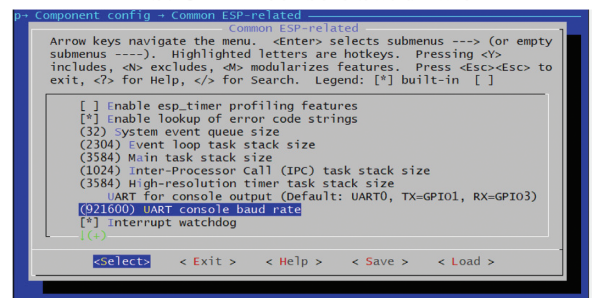
Wi-ESP, as a CSI measurement tool based on ESP32, needed to be set up during the installation process to measure CSI values efficiently. A series of steps were involved to instigate the CSI measuring process (The figures are available for further reference at: <https://github.com/wrlab/Wi-ESP/tree/master/Figures>). These are explained in Wi-Esp (2020) as described below and shown in Fig. 7.

- CPU frequency: Different CPU frequencies of 80, 160, or 240 MHz are available in Wi-ESP. The frequency was set to 240 MHz to measure CSI values, as shown in Fig. 7a. The power consumption of Wi-ESP depends on the CPU frequency.
- UART console baud rate: The baud rate is the rate at which Wi-ESP transfers information to the acquiring device. The baud rate was set to a maximum of 921 600 bps in Wi-ESP for recording CSI measurements, as shown in Fig. 7b.

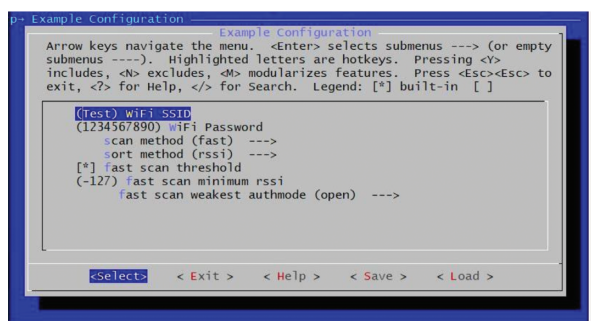
a. Processor clock rate



b. UART console baud rate



c. SSID Information



d. CSI Gathering

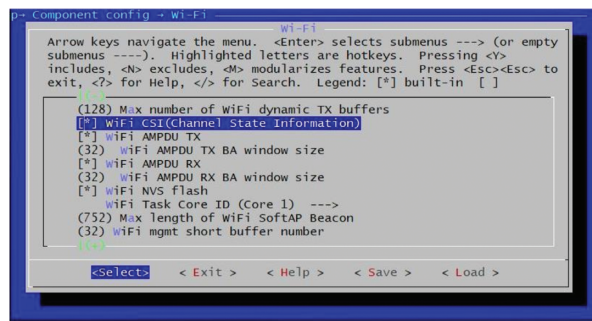


Figure 7: Wi-ESP Settings.

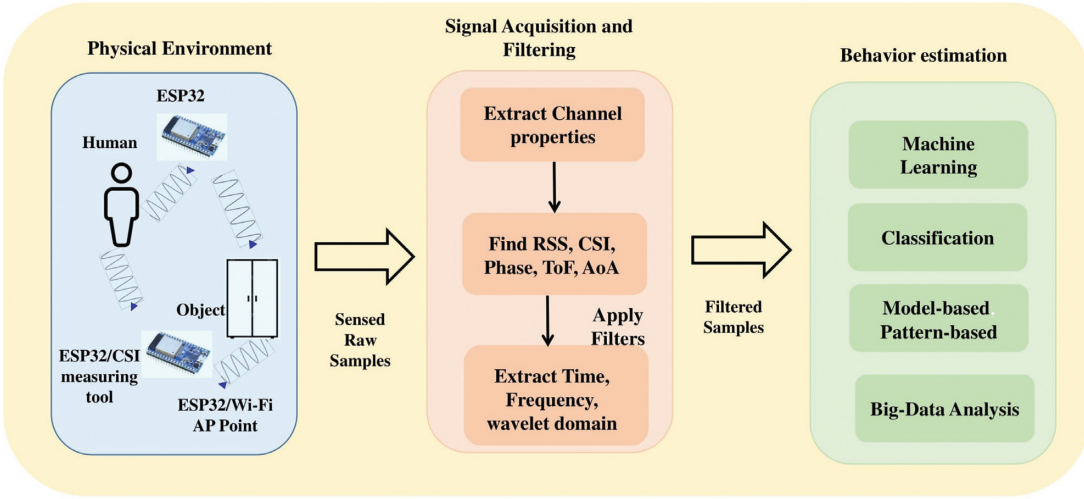


Figure 8: Wi-ESP architecture for DFWS.

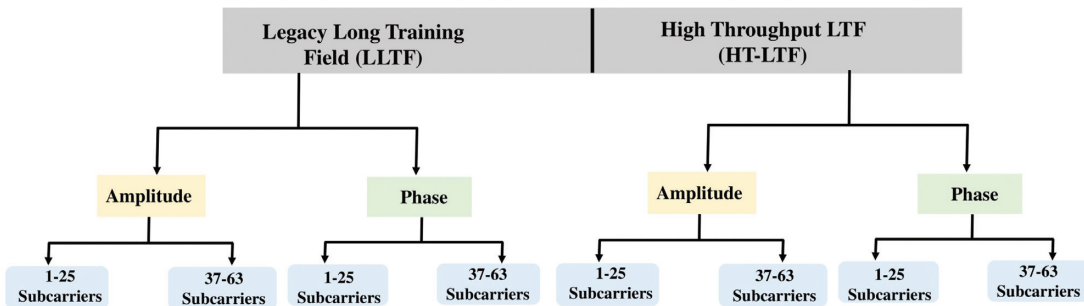


Figure 9: Different training fields in simulation.

- **Wi-Fi setting:** The next step was to tune for Wi-Fi. The Wi-Fi driver uses APIs to initialize Wi-Fi and handles Wi-Fi events by receiving API calls. It communicates the events to the application as shown in Fig. 7c. A password needed to be set up for Wi-Fi for the particular device.
- **CSI settings:** The CSI settings needed to be initialized in Wi-ESP. The ability to receive the CSI values for a particular Wi-Fi channel needed to be enabled during the setup phase, as shown in Fig. 7d.

After setting up the initial parameters, we have used Wi-ESP to measure CSI values under different training fields for both amplitude and phase. The training fields included an LLTF and HT-LTF. The setup for our experiments included an AP, client, and an interceptor, and all of the nodes were Wi-ESP devices. When using Wi-ESP for CSI measurements, we did not need any special devices as RX, but the interceptor needed to be a Wi-ESP. Other nodes such as the AP, server, or client could be commercial devices. After our initial setup and the experimental setup, we evaluated the use of Wi-ESP as a tool for measuring CSI values for DFWS.

4.1. Amplitude and phase of CSI measurements from LLTF

CSI constitutes two information, amplitude and phase. The performance evaluation for Wi-ESP was carried out for LLTF

and HT-LTF. The main purpose of evaluating both fields was to analyze the amplitude and phase signal levels received from both the fields. Each field can support different DFWS applications based on their received CSI values. In the first set of experiments, we measured the amplitude and phase of the CSI values from LLTF. We set ESP32 as a TX and RX without any devices. Figure 8 shows the entire setup for our experiments. The LLTF OFDM symbol in 802.11n is identical to the 802.11a long training OFDM symbol. The results observed were recorded in the same order, as shown in Fig. 9. The LLTF was Binary Phase Shift Keying (BPSK) modulated at 6 Mbps with no channel coding and scrambling. Figure 10 clearly shows the amplitudes of CSI values for all the subcarriers from 1 to 63. Figure 10 shows that out of 63 subcarriers, 52 subcarriers were active and the rest were inactive (The figures are available for further reference at: <https://github.com/wrlab/Wi-ESP/tree/master/Figures>). Furthermore, each subcarrier shows different signal levels that can be exploited for various DFWS applications.

In a few of the subcarriers, no amplitude values were received. We know that the FFT used in the OFDM has a basic requirement that the number of inputs must be 2^n . There were 48 data subcarriers, and 4 subcarriers were used for beacons, so the total number of subcarriers fed to the IFFT was 52. To make the number 2^n , we needed to add 12 more subcarriers, which are shown as 0 in Fig. 10. Using this modification, we could create 64 subcarriers on the transmitter side. On the re-

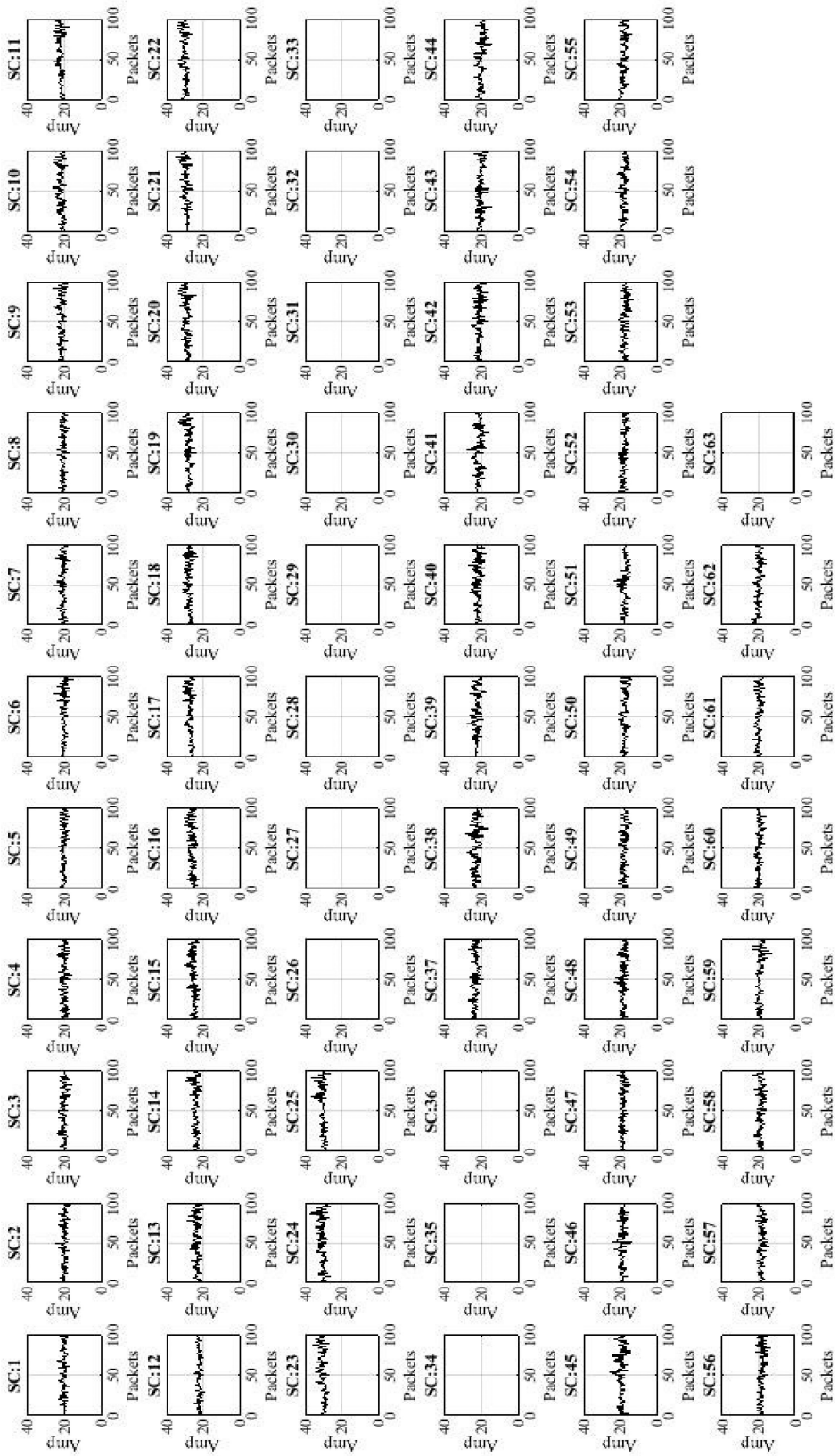


Figure 10: A multiplex from CS1 through all subscenarios 1 to 63 (LTf).

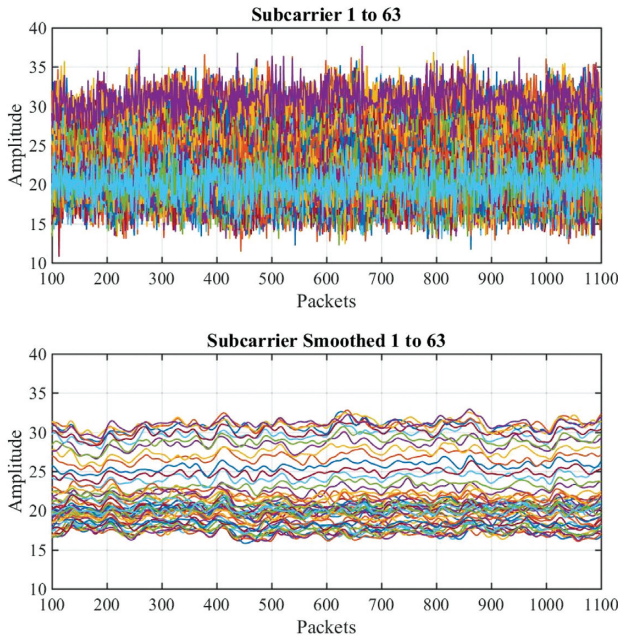


Figure 11: Smoothed amplitude from CSI through 1 to 63 subcarriers (LLTF).

ceiver side, 64 subcarriers were received, and we took an FFT of the signal. Of the 64 subcarriers received, only 52 were active subcarriers; the rest of the data were 0 even though they were active. We received the CSI amplitude from all the 63 subcarriers with the Wi-ESP tool, unlike the other existing CSI tools. Figure 10 shows that the observed amplitude for all the subcarriers is not the same. Different DFWS applications can exploit the amplitude values based on the signal level to serve their particular purpose. For example, a DFWS application detecting motion may be able to use low signal levels, while an application monitoring breathing rate may require high signal levels.

Figure 11 shows the amplitude received from all subcarriers in one figure, smoothed with the help of a Gaussian filter. The Gaussian smoothing filter is a 2D convolution operator that helps to remove detail and noise. After removing the noise, Fig. 11 gives a detailed view of amplitude received from all the subcarriers. Figs 12 and 13 illustrate the amplitudes received in more detail for subcarriers 1 to 25 and 37 to 63, respectively. From the above figures, we can see a clear variation in the received amplitude levels.

To evaluate the next scenario, we measured the phase values obtained from CSI for the LLTF training field. Figure 14 and 15 shows the phase values received from the Wi-ESP CSI tool from subcarriers 1 to 63. Similar to the amplitude measurements, subcarriers 26 to 36 do not show any values (The figures are available for further reference at: <https://github.com/wrlab/Wi-ESP/tree/master/Figures>). The amplitude and phase values received from the entire set of subcarriers can provide precise CSI values useful for various DFWS applications. The other existing CSI tools have random phase values from CSI and need correction for DFWS applications. The phase values received from all subcarriers also show different signal strengths, enabling them to be used for different DFWS applications based on requirements. The shortcomings in existing tools hinder the practical implementation of DFWS applications on a large scale. The Wi-ESP

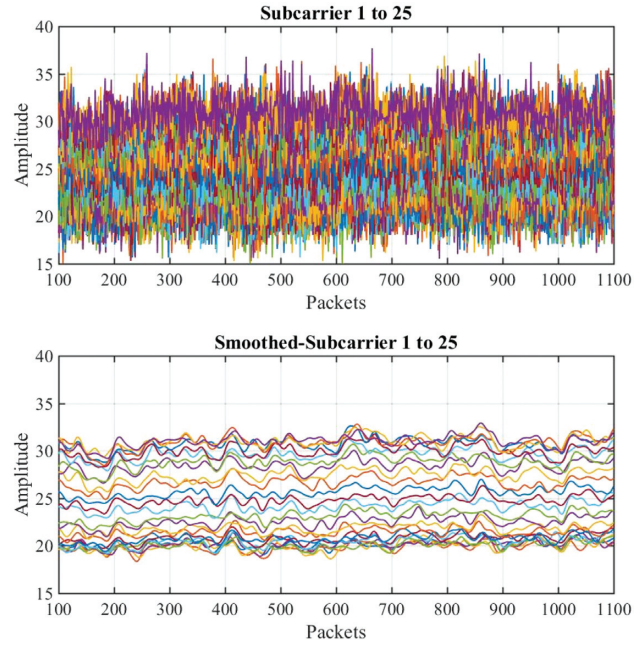


Figure 12: Smoothed amplitude from CSI through 1 to 25 subcarriers (LLTF).

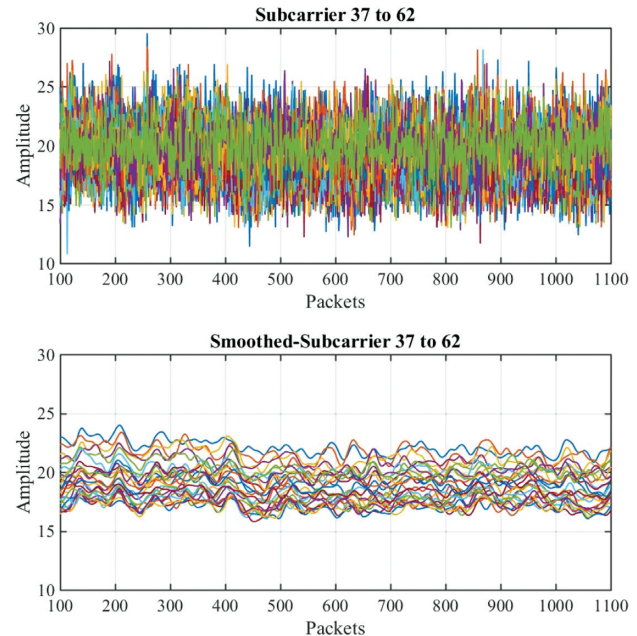


Figure 13: Smoothed amplitude from CSI through 37 to 63 subcarriers (LLTF).

CSI tool is less expensive, and its standalone feature for recording and processing CSI values makes it easier for DFWS application implementation on a large scale.

4.2. Amplitude and phase of CSI measurements from HT-LTF

The HT-LTF provides a means for the RX to estimate the channel between each spatial mapper input (or spatial stream TX

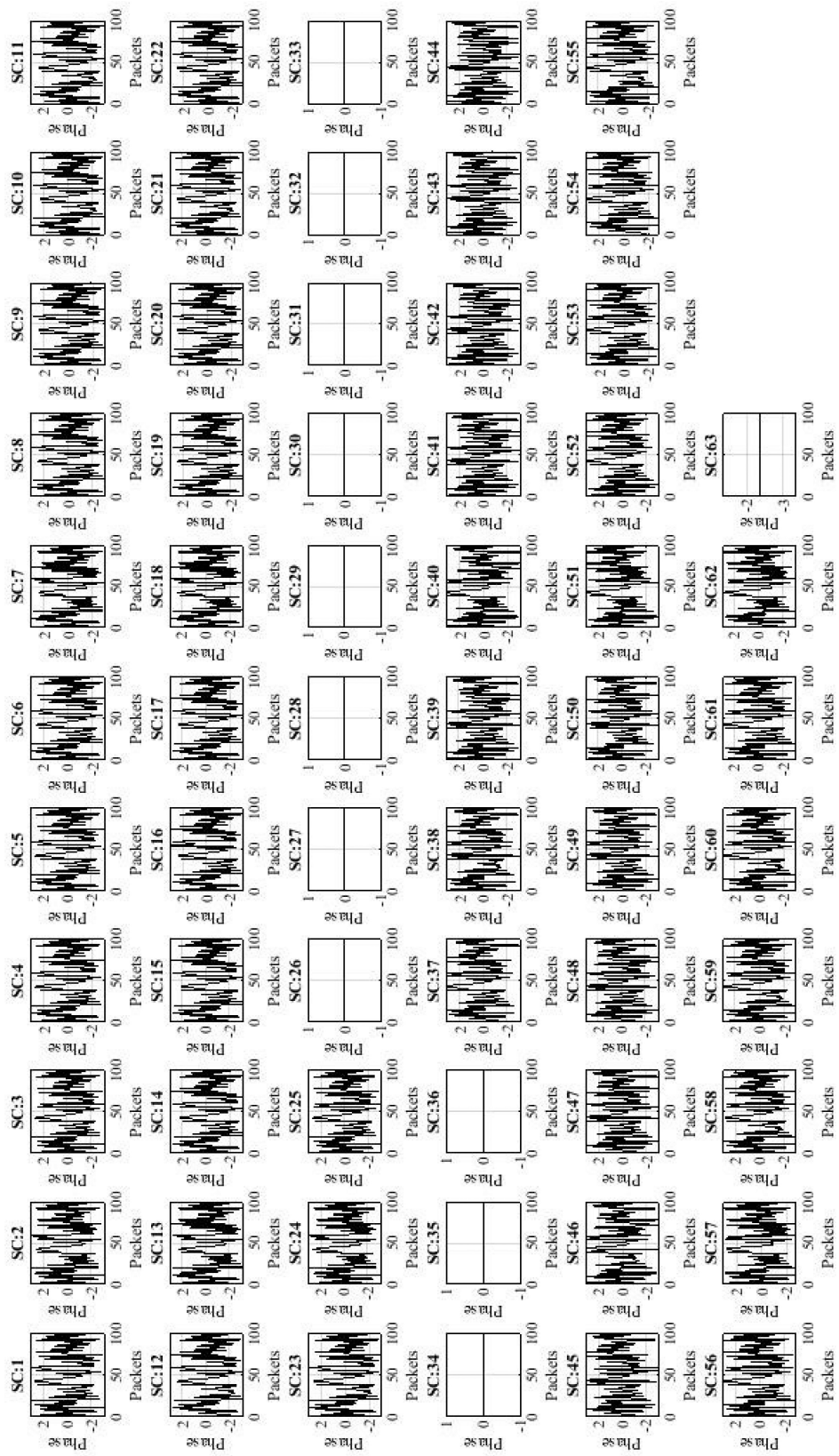


Figure 14: Phase from CS through all subcarriers 1 to 63 (LTU).

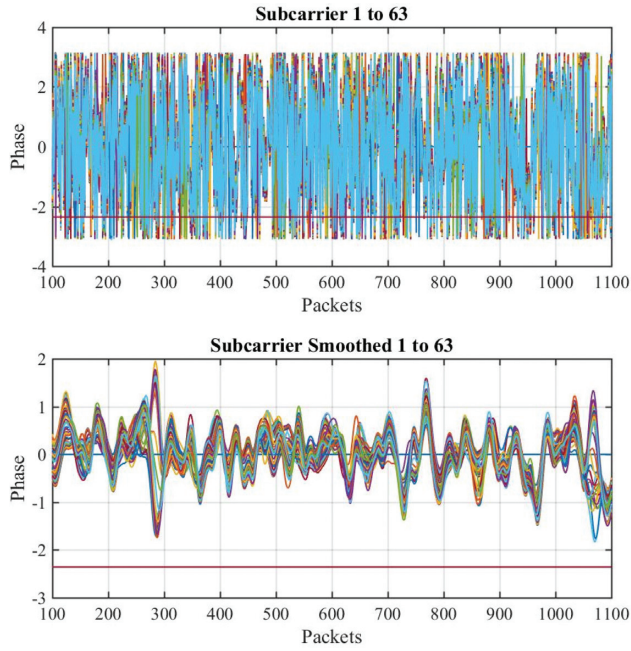


Figure 15: Phase from CSI through subcarriers 1 to 63 (LLTF).

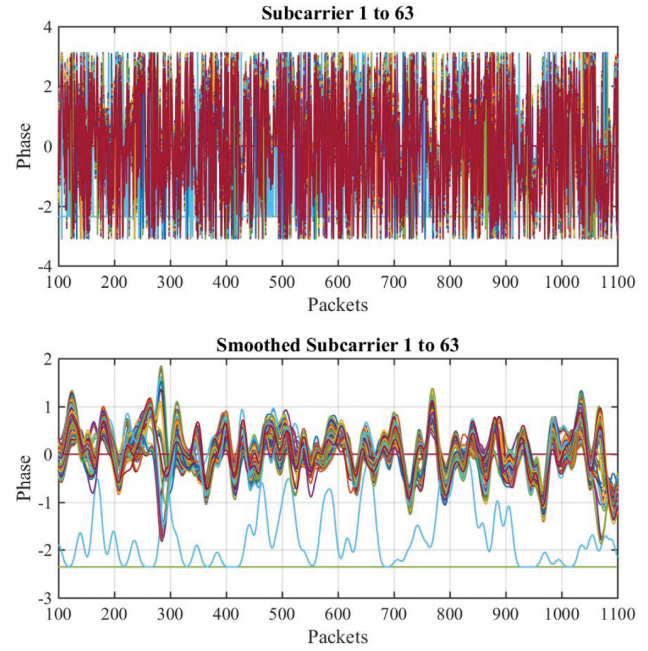


Figure 17: Phase from CSI through subcarriers 1 to 63 (HT-LTF).

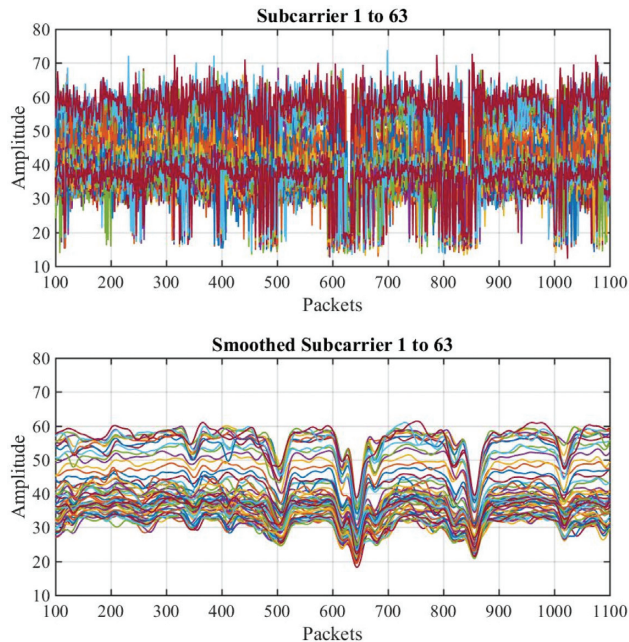


Figure 16: Amplitude from CSI through 1 to 63 subcarriers (HT-LTF).

if no STBC is applied) and receive chain. The number of training symbols is equal to or higher than the number of space-time streams. Similar to LLTF, we received CSI information based on amplitude and phase in all the subcarriers in HT-LTF. Figure 16 depicts the amplitude values from subcarriers 1

to 63 in HT-LTF and the smoothed values after using Gaussian filters.

After measuring the amplitude values, we annotated the phase values from CSI, from the HT-LTF training field. Figure 17 highlights the phase values from CSI after using Gaussian smoothing to smooth out the signal. The phase information from existing CSI tools is significantly affected by random noise and is not usable for applications such as localization or certain other specialized applications such as breath-rate monitoring (Dang, Si, Hao, & Huang, 2019). The phase information from the Wi-ESP CSI tool is not random, since it receives values from all subcarriers, and can be useful for the DFWS applications mentioned above, and many others. Table 2 shows a comparison of current existing CSI tools and Wi-ESP-based CSI tools.

5. Conclusion

We have proposed a Wi-ESP CSI tool for DFWS applications. The Wi-ESP CSI tool has considerable advantages over existing CSI tools and is suitable for practical implementations. The amplitude and phase received from CSI values in Wi-ESP are not random since data are from all 52 subcarriers. The hardware and software dependency of the Wi-ESP CSI tool is much less than other CSI tools. The Wi-ESP CSI tool is flexible, low cost, and easy to deploy as an edge device in large implementations such as IoT. Furthermore, different training fields available in Wi-ESP allow it to receive CSI values for specific applications like breath-rate monitoring and localization with precision. In the future, we will focus on using CSI values for specific DFWS applications.

Table 2: Comparison between existing CSI tools and Wi-ESP.

Features	Intel 5300	Atheros	Wi-ESP
CSI values from subcarriers	30 (Yang et al., 2013)	52	52
Phase information from CSI	Random (Zhuo et al., 2017)	Random (Zhuo et al., 2017)	Usable phase values
Deployment scale	Small scale	Small scale	Large scale
Cost of deployment	High cost (Tzur et al., 2015; Xie et al., 2018)	High cost (Tzur et al., 2015; Xie et al., 2018)	Low cost (Espressif, 2020)
Applications	Used for certain applications (Dang et al., 2019)	Used for certain applications (Dang et al., 2019)	Applicable to any type of applications
Practical implementation	Not possible (Yang et al., 2018)	Not possible (Yang et al., 2018)	Possible
Software dependency	High	High	Low
Flexible architecture	No	No	Yes
Standalone edge device	No	No	Yes
Transmitter (TX)	Computer, laptop, or any commercial devices	Computer, laptop, or any commercial devices	ESP32, computer, laptop, or any commercial devices
Receiver (RX)	Computer, laptop, or any commercial devices	Computer, laptop, or any commercial devices	ESP32, computer, laptop, or any commercial devices
Interceptor	Computer, laptop, or any commercial devices	Computer, laptop, or any commercial devices	ESP32

Acknowledgements

This work was supported by the Korea Institute of Science and Technology (KIST) under the Institutional Program (Grant No. 2E30270).

Conflict of interest statement.

Declarations of interest: none

REFERENCES

- Al-qaness, M. A., Abd Elaziz, M., Kim, S., Ewees, A. A., Abbasi, A. A., Alhaj, Y. A., & Hawbani, A., (2019). Channel state information from pure communication to sense and track human motion: A survey. *Sensors*, 19(15), 3329.
- Bhartia, A., Chen, Y. C., Rallapalli, S., & Qiu, L., (2011). Harnessing frequency diversity in Wi-Fi networks. In *Proceedings of the 17th Annual International Conference on Mobile Computing and Networking*(pp. 253–264), New York, ACM.
- Cho, Y. S., Kim, J., Yang, W. Y., & Kang, C. G., (2010). MIMO-OFDM wireless communications with MATLAB, New Jersey, United States: John Wiley & Sons.
- Choi, J. S., Lee, W. H., Lee, J. H., Lee, J. H., & Kim, S. C., (2017). Deep learning based NLOS identification with commodity WLAN devices. *IEEE Transactions on Vehicular Technology*, 67(4) 3295–3303.
- Dang, X., Si, X., Hao, Z., & Huang, Y., (2019). A novel passive indoor localization method by fusion CSI amplitude and phase information. *Sensors*, 19(4), 875.
- Duan, S., Yu, T., & He, J., (2018). Widriver: Driver activity recognition system based on Wi-Fi CSI. *International Journal of Wireless Information Networks*, 25(2), 146–156.
- ESP-IDF Programming Guide, (2020). <https://docs.espressif.com/projects/esp-idf/en/latest/api-guides/wifi.html?highlight=channel>. (Last Accessed 3 March 2020).
- Espressif, (2020). <https://www.espressif.com/en/products/hardware/esp32/overview/Accessed>. (13 January 2020, date last accessed).
- Gong, L., Yang, W., Zhou, Z., Man, D., Cai, H., Zhou, X., & Yang, Z., (2016). An adaptive wireless passive human detection via fine-grained physical layer information. *Ad Hoc Networks*, 38, 38–50.
- Halperin, D., Hu, W., Sheth, A., & Wetherall, D., (2011a). Predictable 802.11 packet delivery from wireless channel measurements. *ACM SIGCOMM Computer Communication Review*, 41(4) 159–170.
- Halperin, D., Hu, W., Sheth, A., & Wetherall, D., (2011b). Tool release: Gathering 802.11n traces with channel state information. *ACM SIGCOMM Computer Communication Review*, 41(1), 53.
- IEEE 802.11 Working Group, (2016). IEEE standard for information technology—Telecommunications and information exchange between systems—Local and metropolitan area networks—Specific requirements—Part 11: Wireless LAN medium access control (MAC) and physical layer (PHY) specifications amendment 6: Wireless access in vehicular environments. *IEEE Std 802.11*.
- Jiang, X., Zimu, Z., Youwen, Y., & Lionel, M. N., (2016). A survey on wireless indoor localization from the device perspective. *ACM Computing Surveys*, 49(2), 1–31.
- Khalili, A. M., Soliman, A. H., Asaduzzaman, M., & Griffiths, A., (2020). Wi-Fi sensing: Applications and challenges, *The Journal of Engineering*, 2020 (3), 87–97.
- Ma, Y., Zhou, G., & Wang, S., (2019). WiFi sensing with channel state information: A survey. *ACM Computing Surveys (CSUR)*, 52(3), 46.
- Ren, S., Wang, H., Gong, L., Xiang, C., Wu, X., & Du, Y., (2019). Intelligent contactless gesture recognition using WLAN physical layer information. *IEEE Access*, 7, 92758–92767.
- Savazzi, S., Sigg, S., Nicoli, M., Rampa, V., Kianoush, S., & Spagnolini, U., (2016). Device-free radio vision for assisted living: Leveraging wireless channel quality information for human sensing. *IEEE Signal Processing Magazine*, 33(2), 45–58.
- Sen, S., Lee, J., Kim, K. H., & Congdon, P., (2013). Avoiding multipath to revive inbuilding WiFi localization. In *Proceeding of the 11th Annual International Conference on Mobile Systems, Applications, and Services*, (pp. 249–262).
- Tse, D., & Viswanath, P., (2005). *Fundamentals of wireless communication*. New York: Cambridge University Press.
- Tzur, A., Amrani, O., & Wool, A., (2015). Direction finding of rogue Wi-Fi access points using an off-the-shelf MIMO-OFDM receiver. *Physical Communication*, 17, 149–164.

- Wang, Y., Wu, K., & Ni, L. M., (2016). Wifall: Device-free fall detection by wireless networks. *IEEE Transactions on Mobile Computing*, 16(2), 581–594.
- Wang, Z., Guo, B., Yu, Z., & Zhou, X., (2018). Wi-Fi CSI-based behavior recognition: From signals and actions to activities. *IEEE Communications Magazine*, 56(5), 109–115.
- Wang, Z., Jiang, K., Hou, Y., Dou, W., Zhang, C., Huang, Z., & Guo, Y., (2019). A survey on human behavior recognition using channel state information. *IEEE Access*, 7, 155986–156024.
- Wengrowski, E., (2014). A survey on device-free passive localization and gesture recognition via body wave reflections. *ACM Transactions on Autonomous and Adaptive Systems*, 5, 1–15.
- Wi-Esp, (2020). <https://github.com/wrlab/Wi-ESP.git/Accessed>. (4 February 2020, date last accessed).
- Woyach, K., Puccinelli, D., & Haenggi, M., (2006). Sensorless sensing in wireless networks: Implementation and measurements. In *n 2006 4th International Symposium on Modeling and Optimization in Mobile, Ad Hoc and Wireless Networks*(pp. 1–8).
- Wu, D., Zhang, D., Xu, C., Wang, H., & Li, X., (2017). Device-free WiFi human sensing: From pattern-based to model-based approaches. *IEEE Communications Magazine*, 55(10), 91–97.
- Xie, Y., Li, Z., & Li, M., (2018). Precise power delay profiling with commodity Wi-Fi. *IEEE Transactions on Mobile Computing*, 18(6), 1342–1355.
- Xin, T., Guo, B., Wang, Z., Wang, P., Lam, J. C. K., Li, V., & Yu, Z., (2018). Freesense: a robust approach for indoor human detection using Wi-Fi signals. *Proceedings of the ACM on Interactive, Mobile, Wearable and Ubiquitous Technologies*, 2(3), 1–23.
- Yang, Z., Zhou, Z., & Liu, Y., (2013). From RSSI to CSI: Indoor localization via channel response. *ACM Computing Surveys (CSUR)*, 46(2), 25.
- Yang, J., Zou, H., Jiang, H., & Xie, L., (2018). Device-free occupant activity sensing using WiFi-enabled iot devices for smart homes. *IEEE Internet of Things Journal*, 5(5), 3991–4002.
- Yousefi, S., Narui, H., Dayal, S., Ermon, S., & Valaei, S., (2017). A survey on behavior recognition using WiFi channel state information. *IEEE Communications Magazine*, 55(10), 98–104.
- Youssef, M., Mah, M., & Agrawala, A., (2007). Challenges: Device-free passive localization for wireless environments. In *Proceedings of the 13th Annual ACM International Conference on Mobile Computing and Networking*(pp. 222–229).
- Zhang, D., Wang, H., & Wu, D., (2017). Toward centimeter-scale human activity sensing with Wi-Fi signals. *Computer*, 50(1), 48–57.
- Zhang, L., Liu, M., Lu, L., & Gong, L., (2018). Wi-Run: Multi-runner step estimation using commodity Wi-Fi. In *15th Annual IEEE International Conference on Sensing, Communication, and Networking (SECON)*(pp.1–9).
- Zhao, J., Liu, L., Wei, Z., Zhang, C., Wang, W., & Fan, Y., (2019). R-DEHM: CSI-based robust duration estimation of human motion with WiFi. *Sensors*, 19(6), 1421.
- Zheng, L., Hu, B., & Chen, H., (2018). A high accuracy time-reversal based WiFi indoor localization approach with a single antenna. *Sensors*, 18, 3437.
- Zhou, Z., Wu, C., Yang, Z., & Liu, Y., (2015). Sensorless sensing with WiFi. *Tsinghua Science and Technology*, 20(1), 1–6.
- Zhuo, Y., Zhu, H., & Xue, H., (2016). Identifying a new non-linear CSI phase measurement error with commodity WiFi devices. In *Proceedings of the 2016 IEEE 22nd International Conference on Parallel and Distributed Systems (ICPADS)*(pp. 72–79), Wuhan, China.
- Zhuo, Y., Zhu, H., Xue, H., & Chang, S., (2017). Perceiving accurate CSI phases with commodity WiFi devices. In *IEEE INFOCOM 2017 - IEEE Conference on Computer Communications*(pp. 1–9), Atlanta, GA, USA.
- Zou, H., Zhou, Y., Yang, J., Jiang, H., Xie, L., & Spanos, C. J., (2018). DeepSense: Device-free human activity recognition via autoencoder long-term recurrent convolutional network. In *IEEE International Conference on Communications (ICC)*(pp. 1–6), Kansas City, MO, USA.